Supporting Information

Two (5, 5)-connected isomeric frameworks as highly selective and sensitive photoluminescent probes of nitroaromatics

Yue Dai,[a] Huajun Zhou,[b] Xue-Dan Song,[a] Jian-Jun Zhang,[a] Ce Hao,[a] Ling Di,[a] Yu-Xian Wang,[a] Jun Ni,[a] Hui-Long Wang[a]**

[a] Chemistry College, Dalian University of Technology, Dalian 116024, China

[b] High Density Electronics Center, University of Arkansas, Fayetteville, Arkansas 72701, USA

Table S1. Selected bond lengths (Å) and angles (°) for complex **1**.

Zn(1)-O(9)#1	1.927(4)	Zn(2)-O(2)#4	2.484(4)
Zn(1)-O(5)#2	1.930(4)	O(1)-Zn(2)#4	1.990(4)
Zn(1)-O(8)	1.989(3)	O(2)-Zn(2)#4	2.484(4)
Zn(1)-O(11)	2.132(6)	O(3)-Zn(2)#5	1.996(3)
Zn(1)-O(4)#3	2.163(4)	O(4)-Zn(1)#5	2.163(4)
Zn(2)-O(7)	1.981(4)	O(5)-Zn(1)#2	1.930(4)
Zn(2)-O(1)#4	1.990(4)	O(9)-Zn(1)#6	1.927(4)
Zn(2)-O(3)#3	1.996(3)	O(10)-Zn(2)#6	2.001(4)
Zn(2)-O(10)#1	2.001(4)		
O(9)#1-Zn(1)-O(5)#2	140.69(19)	O(7)-Zn(2)-O(1)#4	111.00(19)
O(9)#1-Zn(1)-O(8)	108.91(18)	O(7)-Zn(2)-O(3)#3	100.71(17)
O(5)#2-Zn(1)-O(8)	110.34(16)	O(1)#4-Zn(2)-O(3)#3	96.32(15)
O(9)#1-Zn(1)-O(11)	85.7(3)	O(7)-Zn(2)-O(10)#1	136.49(17)
O(5)#2-Zn(1)-O(11)	89.9(2)	O(1)#4-Zn(2)-O(10)#1	105.66(19)
O(8)-Zn(1)-O(11)	93.6(2)	O(3)#3-Zn(2)-O(10)#1	97.66(18)
O(9)#1-Zn(1)-O(4)#3	88.6(3)	O(7)-Zn(2)-O(2)#4	91.25(16)
O(5)#2-Zn(1)-O(4)#3	93.87(17)	O(1)#4-Zn(2)-O(2)#4	56.53(15)
O(8)-Zn(1)-O(4)#3	89.29(16)	O(3)#3-Zn(2)-O(2)#4	152.84(13)
O(11)-Zn(1)-O(4)#3	174.1(3)	O(10)#1-Zn(2)-O(2)#4	89.90(17)

Symmetry transformations used to generate equivalent atoms. #1 = -x+1/2, y-1/2, -z; #2 = -x+1, y, -z+1; #3 = x, y, z-1; #4 = -x, y, -z; #5= x, y, z+1; #6 = -x+1/2, y+1/2, -z.

Table S2. Selected bond lengths (Å) and angles (°) for complex **2**.

Zn(1)-O(10)#1	2.000(11)	Zn(2)-O(6)#4	1.923(8)
Zn(1)-O(8)	2.017(7)	Zn(2)-O(7)	1.948(5)
Zn(1)-O(11)	2.126(9)	Zn(2)-O(9)#1	1.976(10)
Zn(1)-O(4)#2	2.147(9)	Zn(2)-O(2)#3	2.032(7)
Zn(1)-O(1)#3	2.171(11)	Zn(2)-O(1)#3	2.352(10)
Zn(1)-O(3)#2	2.196(10)	O(1)-Zn(2)#5	2.352(10)
O(1)-Zn(1)#5	2.171(10)	O(2)-Zn(2)#5	2.032(7)
O(4)-Zn(1)#6	2.147(9)	O(6)-Zn(2)#4	1.923(8)
O(3)-Zn(1)#6	2.196(10)	O(9)-Zn(2)#7	1.976(10)
O(10)-Zn(1)#7	2.000(11)		
O(10)#1-Zn(1)-O(8)	92.1(3)	O(4)#2-Zn(1)-O(3)#2	61.0(3)
O(10)#1-Zn(1)-O(11)	91.5(5)	O(1)#3-Zn(1)-O(3)#2	152.9(3)
O(8)-Zn(1)-O(11)	175.7(6)	O(6)#4-Zn(2)-O(9)#1	107.1(4)
O(10)#1-Zn(1)-O(4)#2	158.3(4)	O(7)-Zn(2)-O(9)#1	104.4(3)
O(8)-Zn(1)-O(4)#2	91.4(3)	O(6)#4-Zn(2)-O(2)#3	110.5(3)
O(11)-Zn(1)-O(4)#2	86.2(5)	O(7)-Zn(2)-O(2)#3	131.8(3)
O(10)#1-Zn(1)-O(1)#3	108.7(4)	O(9)#1-Zn(2)-O(2)#3	107.5(3)
O(8)-Zn(1)-O(1)#3	84.1(3)	O(6)#4-Zn(2)-O(1)#3	153.4(4)
O(11)-Zn(1)-O(1)#3	92.5(6)	O(7)-Zn(2)-O(1)#3	83.1(3)
O(4)#2-Zn(1)-O(1)#3	93.0(4)	O(9)#1-Zn(2)-O(1)#3	99.4(4)
O(10)#1-Zn(1)-O(3)#2	97.7(4)	O(2)#3-Zn(2)-O(1)#3	57.0(3)
O(8)-Zn(1)-O(3)#2	89.1(3)	O(6)#4-Zn(2)-O(7)	93.0(3)
O(11)-Zn(1)-O(3)#2	92.8(5)	Zn(1)#5-O(1)-Zn(2)#5	99.4(4)

Symmetry transformations used to generate equivalent atoms. #1= x, -y+1, z+1/2; #2= -x-1/2, y+1/2, -z-1/2; #3 = x+1/2, -y+1/2, z+1/2; #4= -x-1/2, -y+1/2, -z; #5= x-1/2, -y+1/2, z-1/2; #6 = -x-1/2, y-1/2, -z-1/2; #7 = x, -y+1, z-1/2.

Table S3. A comparison of calculated CB and VB of complexes **1**-**2** and reported complexes based on H_5L^1.

	CB / eV	VB / eV	Band gap / eV
1	-0.4018	-3.6246	3.222
2	-0.9373	-2.6112	1.673
$(Me_2NH_2)[Zn_2L^1]\cdot 3.5DMF$ [1]	-1.3026	-3.9615	2.658
$[Zn_2L^1(H_2O)]\cdot 2DMF\cdot 8H_2O$ [1]	-1.3526	-4.2597	2.907

Methods for DFT calculations:

Density-functional theory (DFT) calculations were carried out by using the Vienna ab-initio simulation package (VASP) code.[2-3] The electron-ion interactions was described by Projector-augmented wave (PAW) potentials,[4]

and the exchange correlation term was treated within the Local density approximation (LDA).[5] All calculations were made with plane-wave cutoff of 520 eV. The convergences of energy and force were set to 1×10^{-4} eV and 0.05 eV/Å, respectively.

References:

[1] L. Di, J.-J. Zhang, S.-Q. Liu, J. Ni, H. Zhou, Y.-J. Sun. Cryst. Growth Des. 16 (2016), 4539–4546.

[2] G. Kresse, J. Furthmüller, Phys. Rev. B 54 (1996) 11169–11186.

[3] G. Kresse, J. Furthmüller, Comput. Mater. Sci. 6 (1996) 15–50.

[4] G. Kresse and D. Joubert, Phys. Rev. B 59, 1758 (1999).

[5] J. P. Perdew, Electronic Structure of Solids (Akademie Verlag, Berlin, 1991).

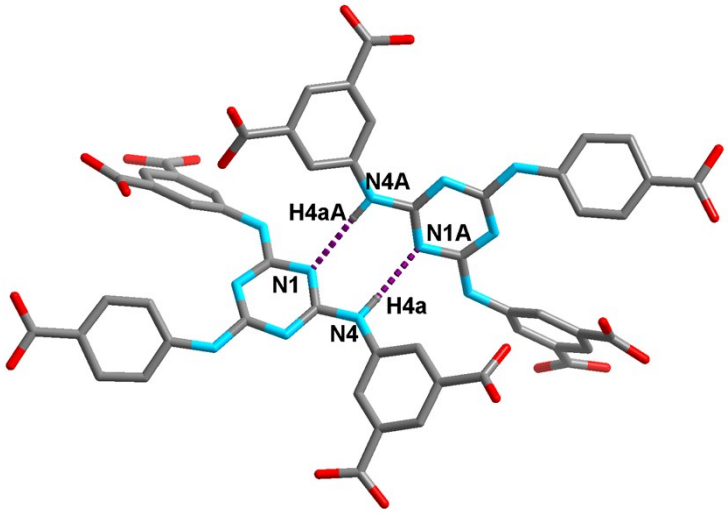

Fig. S1 The hydrogen bonds (represented as dotted line) between neighboring ligands in **1**. Symmetry codes: A = 1 − x, y, 1 – z. (N4···N1A = 3.038 Å, ∠N4-H4a···N1A = 177.08º)

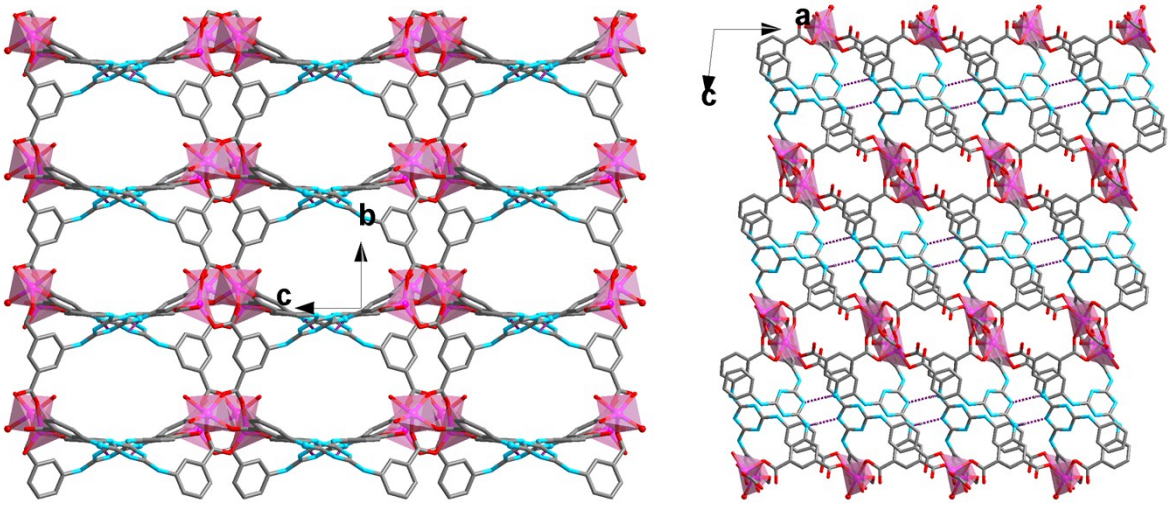

(a) (b)

Fig. S2 The 3D framework of **1** viewed along the *a* direction (a) and *b* direction (b).

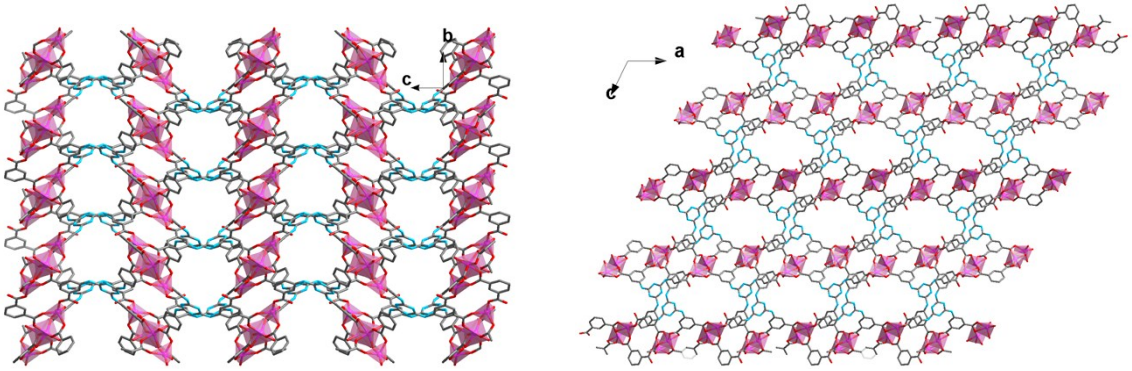

(a) (b)

Fig. S3 The 3D framework of **2** viewed along the *b* axis (a) and *c* axis (b) .

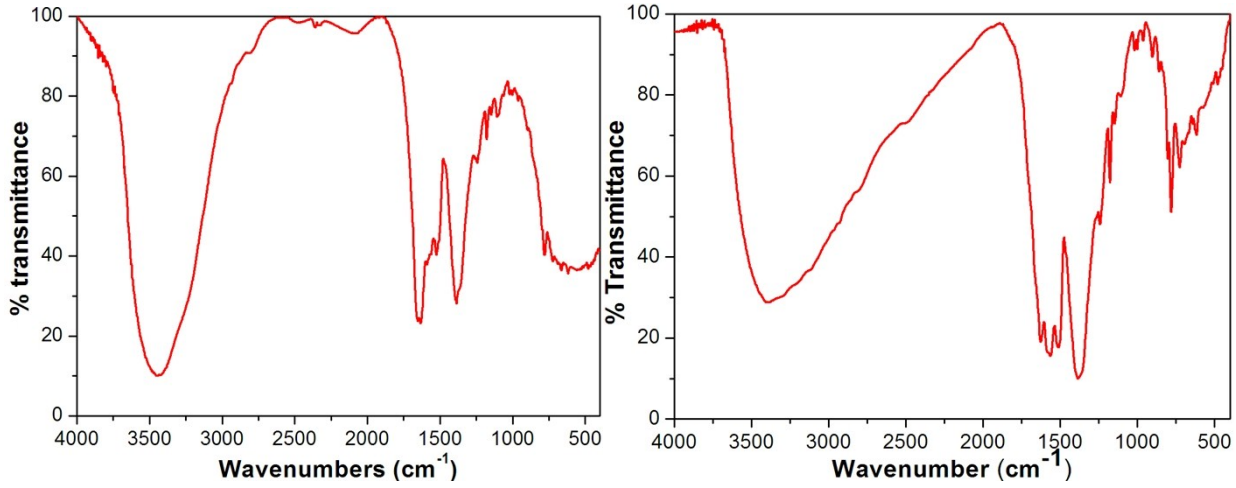

(a) (b)

Fig. S4 IR spectrum of the compound**1** (a) and **2** (b).

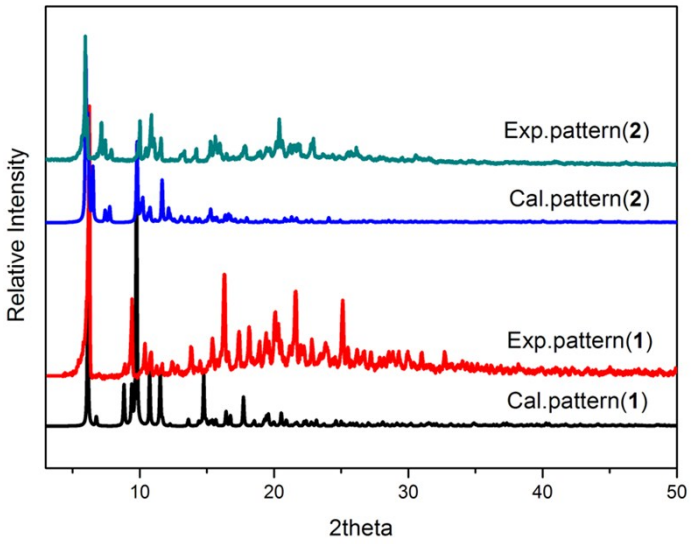

Fig. S5 PXRD patterns of **1**-**2**.

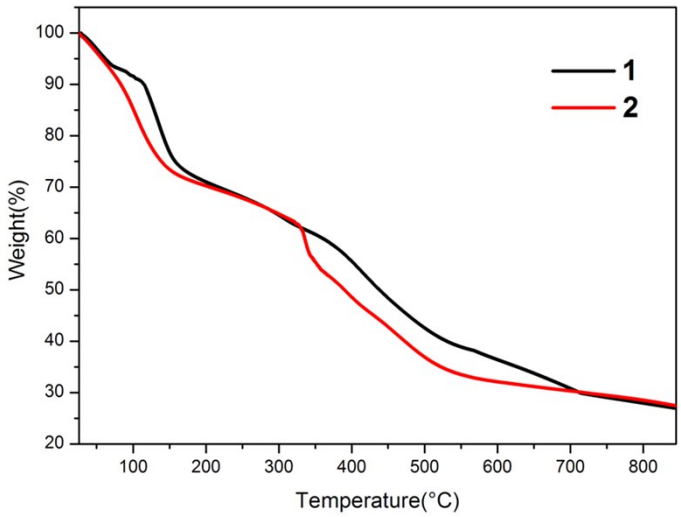

Fig. S6 TGA curves of **1**-**2**.

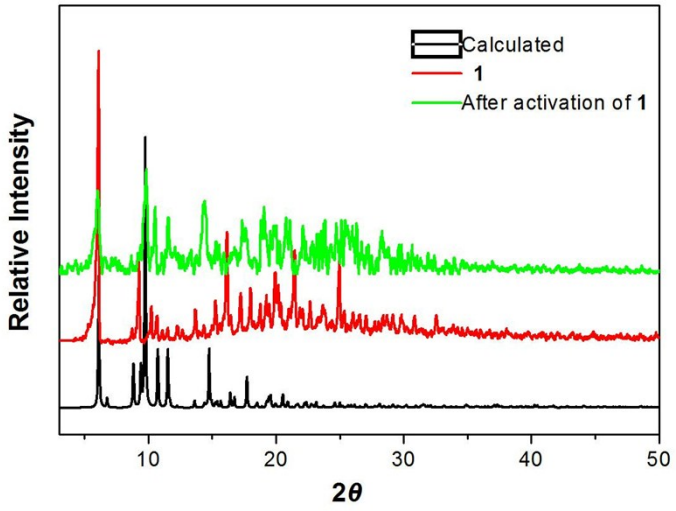

Fig. S7 PXRD patterns of **1** and after activation of **1**.

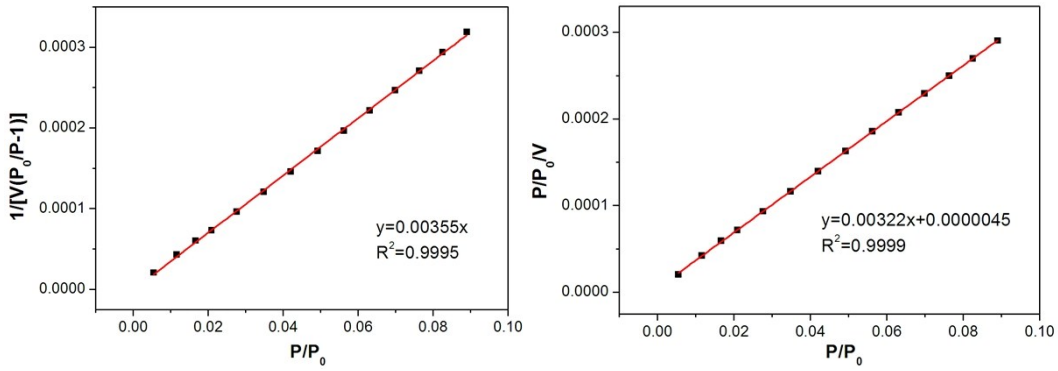

(a) (b)

Fig. S8 Langmuir plot (a) and BET plot (b) of the N_2 isotherm for **1** collected at 77 K.

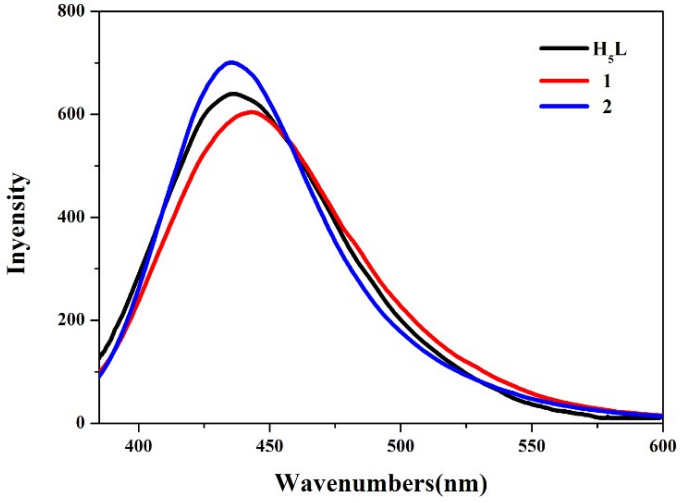

Fig. S9 Solid state PL spectra of ligand H_5L and compounds **1** and **2**, under λ_{ex} = 360 nm.

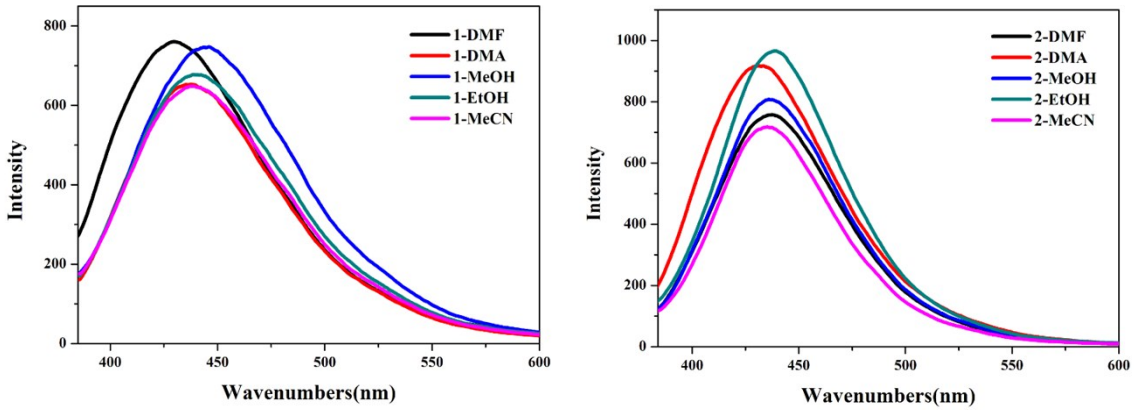

(a) **(b)**

Fig. S10 PL spectra (λ_{ex} = 360 nm) of suspensions of **1** (a) and **2** (b) dispersed in DMF, DMA, MeOH, EtOH and MeCN.

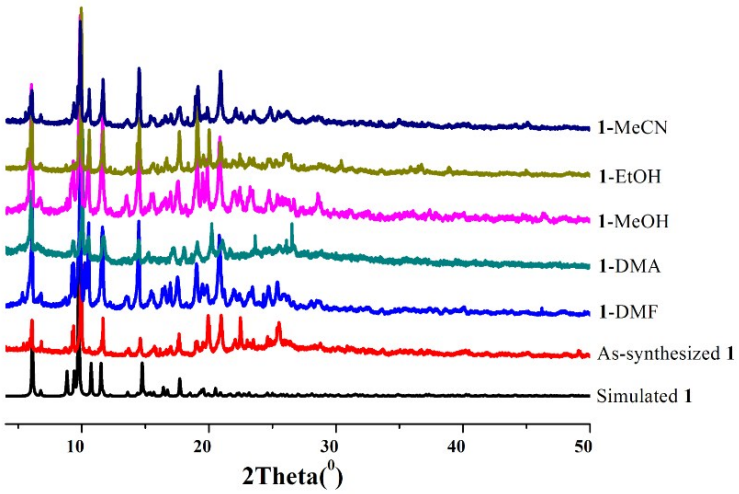

Fig. S11 A comparison of the powder patterns of **1** and products of **1** soaked in different solvents at room temperature.

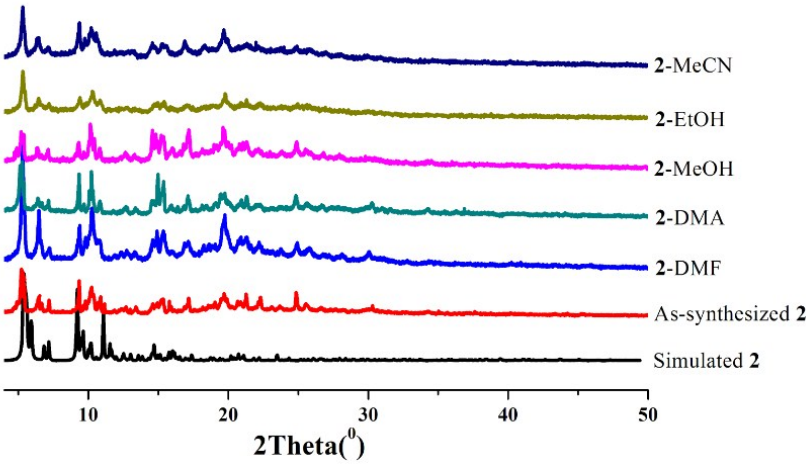

Fig. S12 A comparison of the powder patterns of **2** and products of **2** soaked in different solvents at room temperature.

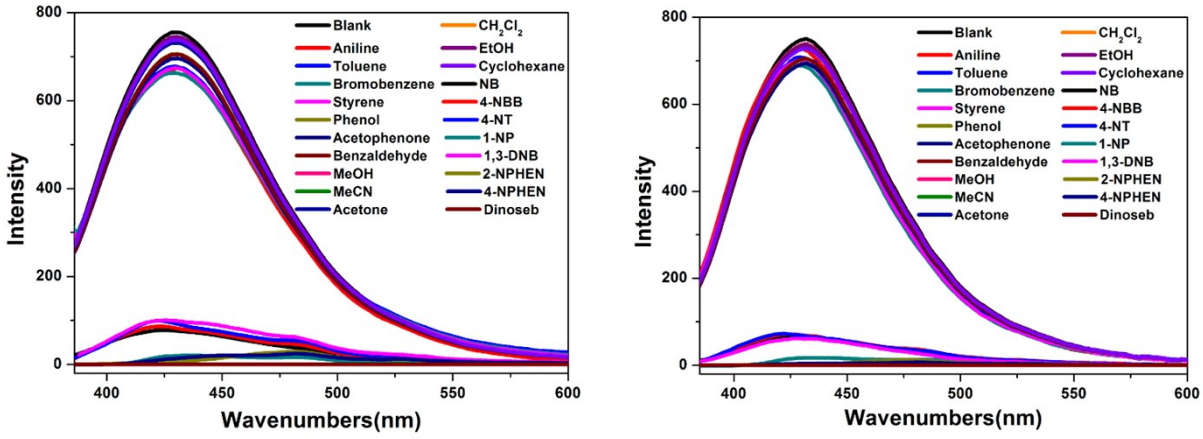

(a) (b)

Fig. S13 PL spectra (λ_{ex} = 360 nm) of **1**(a) and **2**(b) dispersed in 0.01M DMF solutions of different organics.

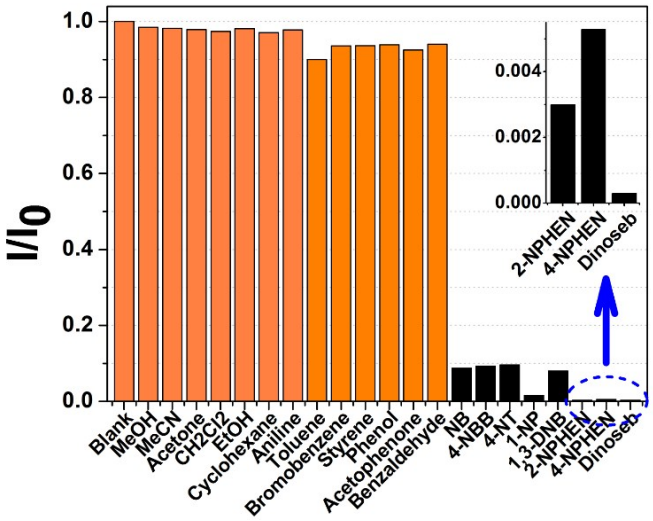

Fig. S14 Fluorescence intensity ratio histograms of suspensions of **2** dispersed in 0.015M DMF solution of different organics.

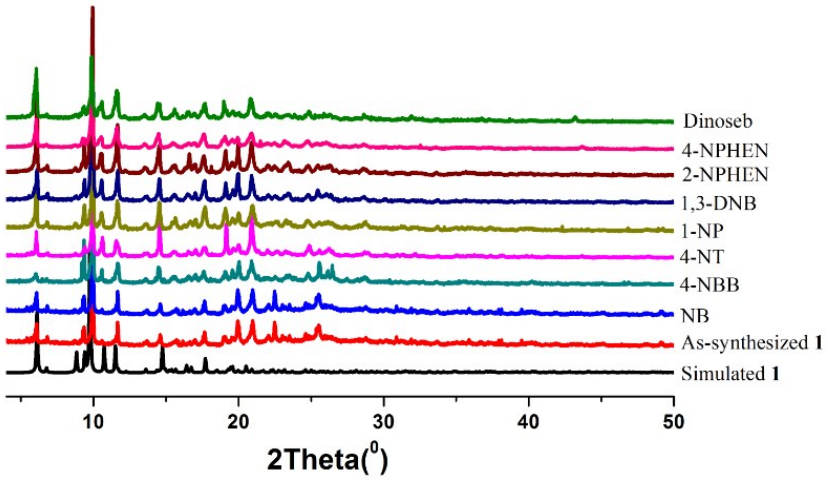

Fig. S15 A comparison of the powder patterns of **1** and products of **1** soaked in DMF solutions containing different NACs at room temperature.

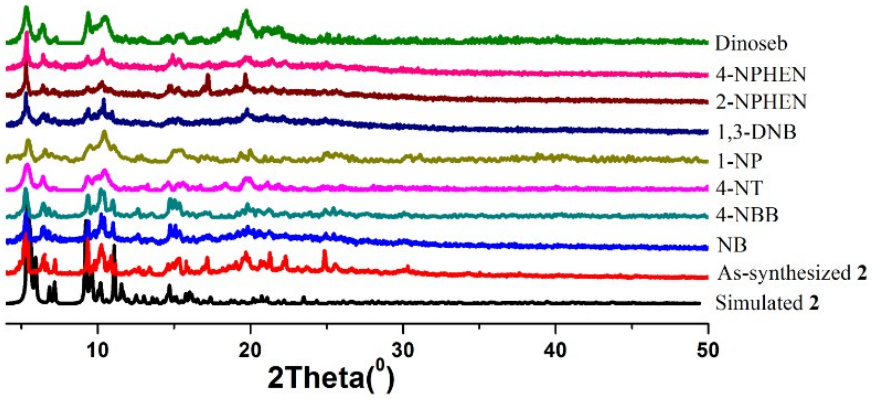

Fig. S16 A comparison of the powder patterns of **2** and products of **2** soaked in DMF solutions containing different NACs at room temperature.

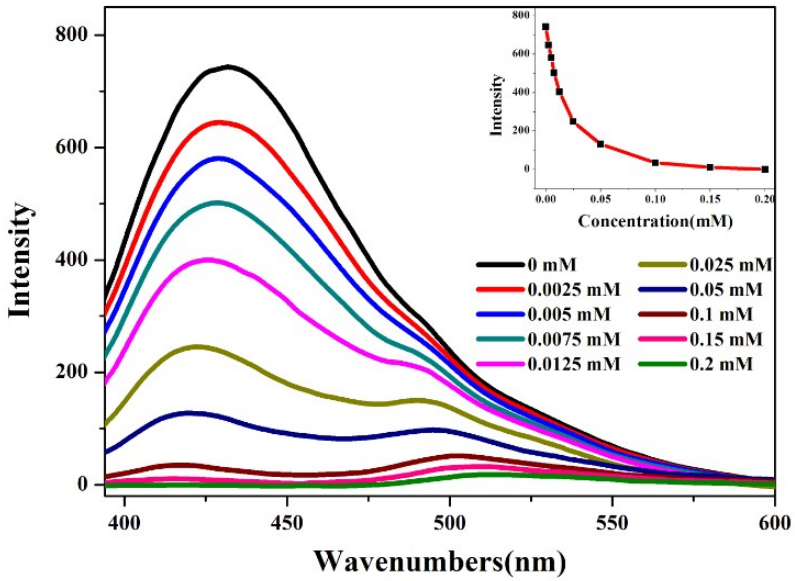

Fig. S17 PL (λ_{ex} = 360 nm) titration of suspensions of **2** (DMF) by gradual addition of dinoseb (insert shows the PL intensity as a function of dinoseb content).

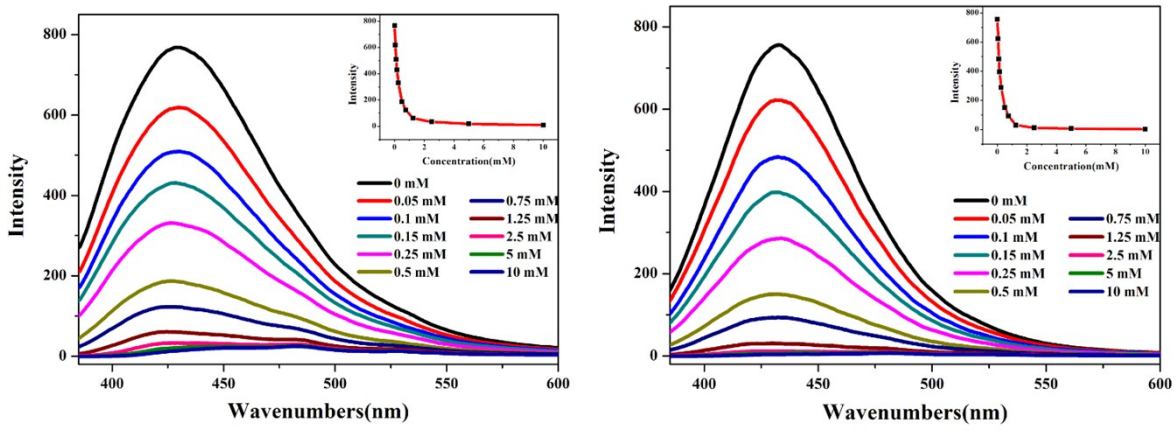

(a) (b)

Fig. S18 PL (λ_{ex} = 360 nm) titration of suspensions of **1** (a) (DMF) and **2** (b) (DMF) by gradual addition of 4-NPPHEN (insert shows the PL intensity as a function of 4-NPPHEN content).

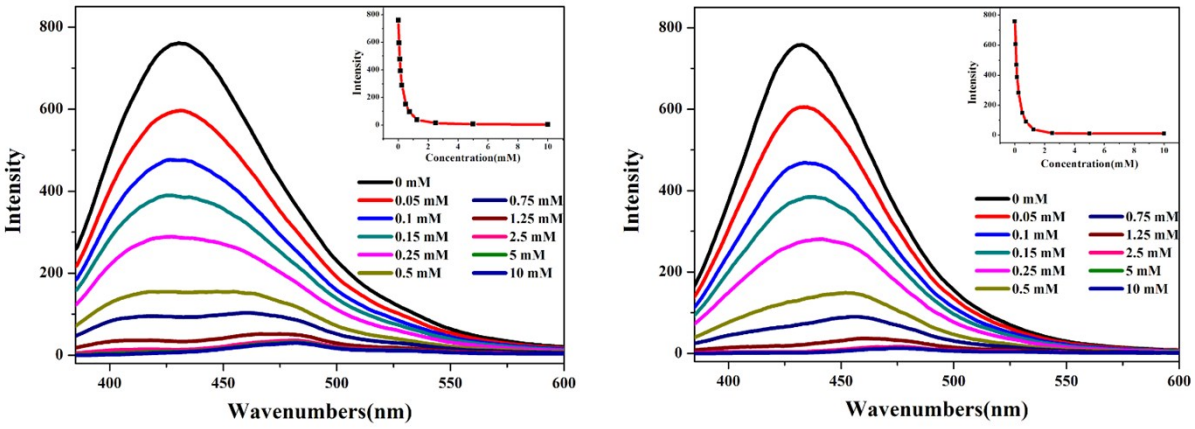

(a) (b)

Fig. S19 PL (λ_{ex} = 360 nm) titration of suspensions of **1** (a) (DMF) and **2** (b) (DMF) by gradual addition of 2-NPPHEN (insert shows the PL intensity as a function of 2-NPPHEN content).

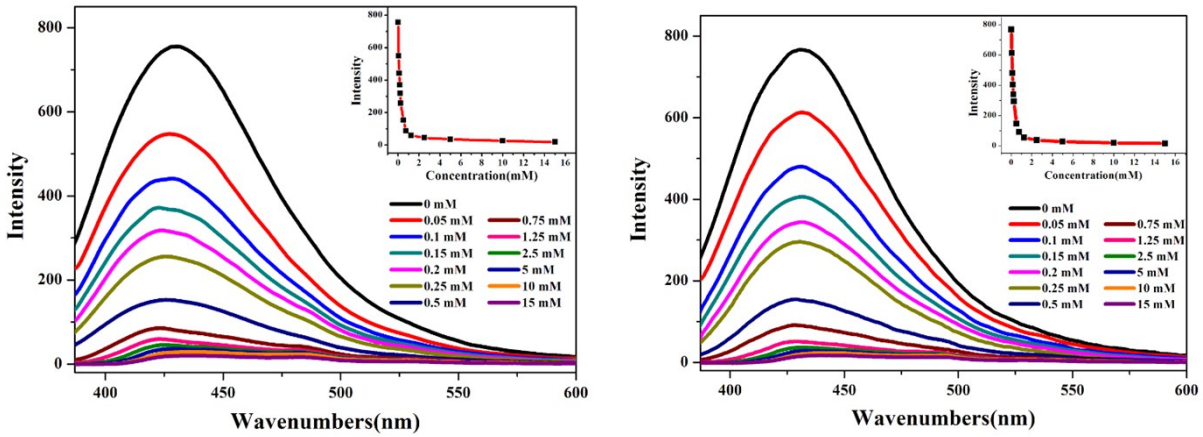

(a) (b)

Fig. S20 PL (λ_{ex} = 360 nm) titration of suspensions of **1** (a) (DMF) and **2** (b) (DMF) by gradual addition of 1-NP (insert shows the PL intensity as a function of 1-NP content).

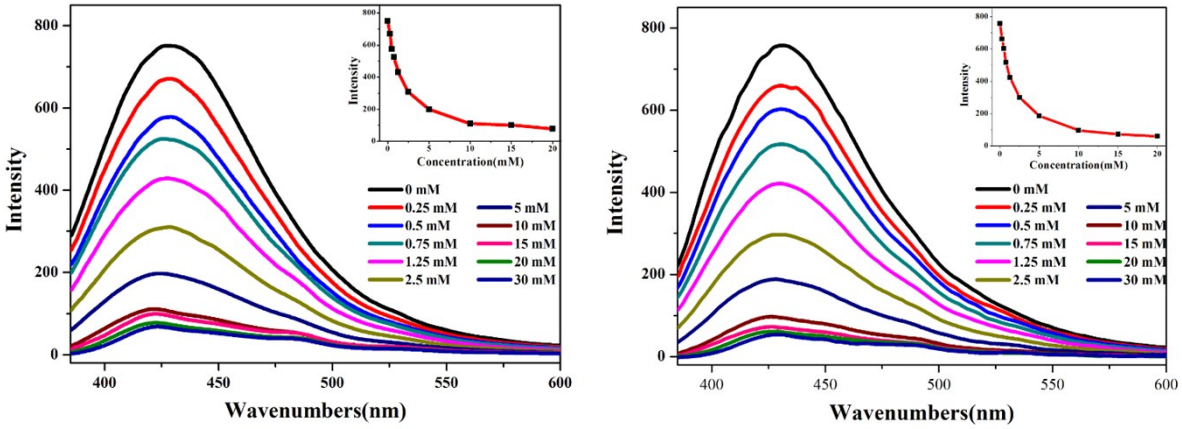

(a) (b)

Fig. S21 PL (λ_{ex} = 360 nm) titration of suspensions of **1** (a) (DMF) and **2** (b) (DMF) by gradual addition of 4-NT (insert shows the PL intensity as a function of 4-NT content).

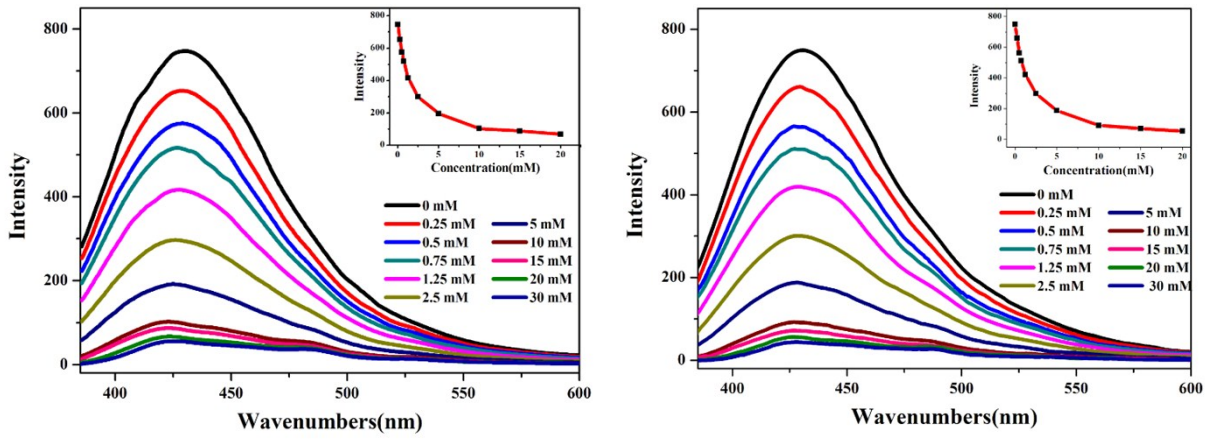

(a) (b)

Fig. S22 PL (λ_{ex} = 360 nm) titration of suspensions of **1** (a) (DMF) and **2** (b) (DMF) by gradual addition of 4-NBB (insert shows the PL intensity as a function of 4-NBB content).

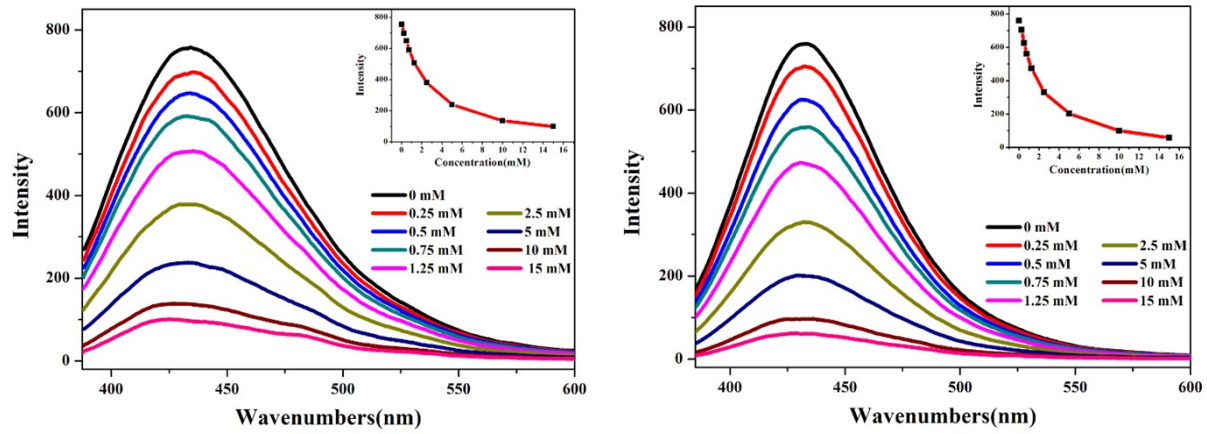

(a) (b)

Fig. S23 PL (λ_{ex} = 360 nm) titration of suspensions of **1** (a) (DMF) and **2** (b) (DMF) by gradual addition of 1,3-DNB (insert shows the PL intensity as a function of 1,3-DNB content).

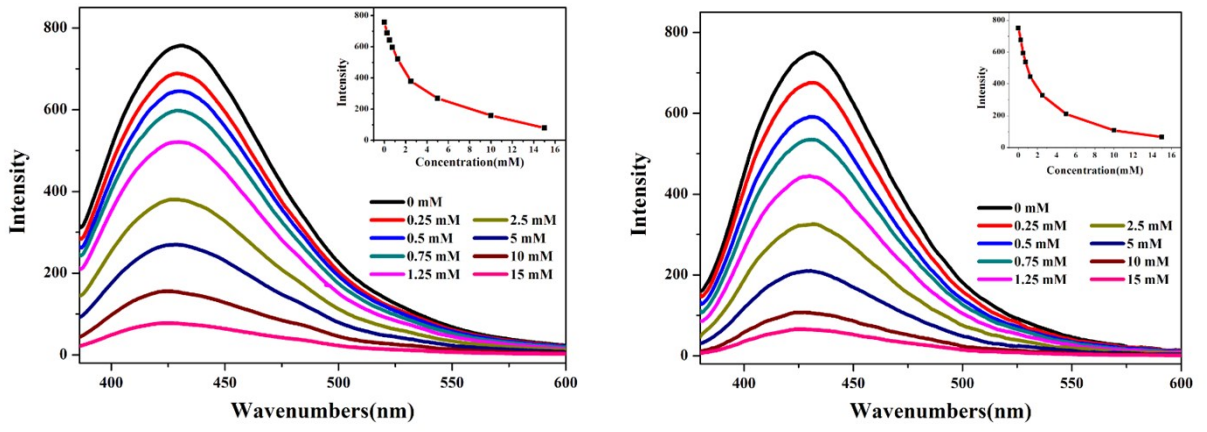

(a) (b)

Fig. S24 PL (λ_{ex} = 360 nm) titration of suspensions of **1** (a) (DMF) and **2** (b) (DMF) by gradual addition of NB (insert shows the PL intensity as a function of NB content).

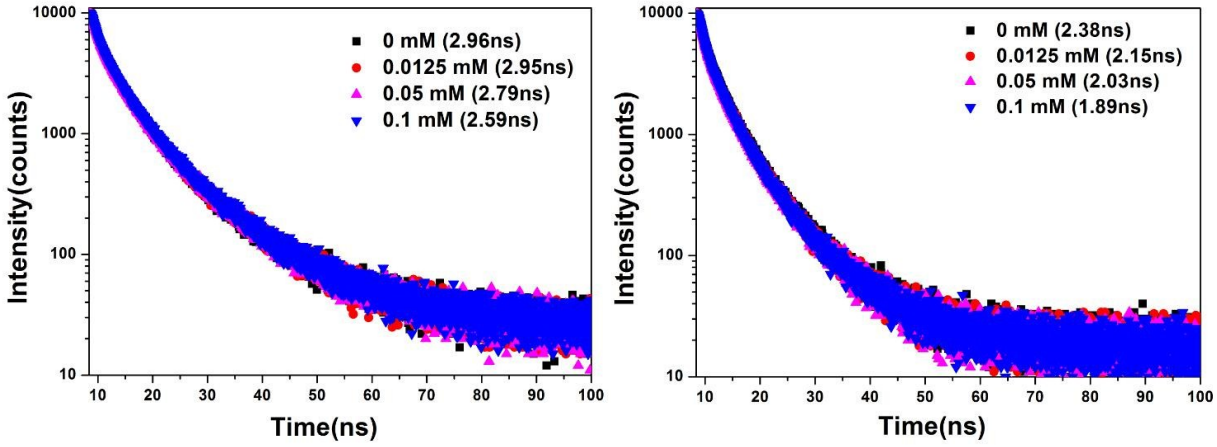

(a) (b)

Fig. S25 Emission decay curves and lifetime of **1** (a) and **2** (b) in DMF suspension upon an incremental addition of dinoseb at room temperature.

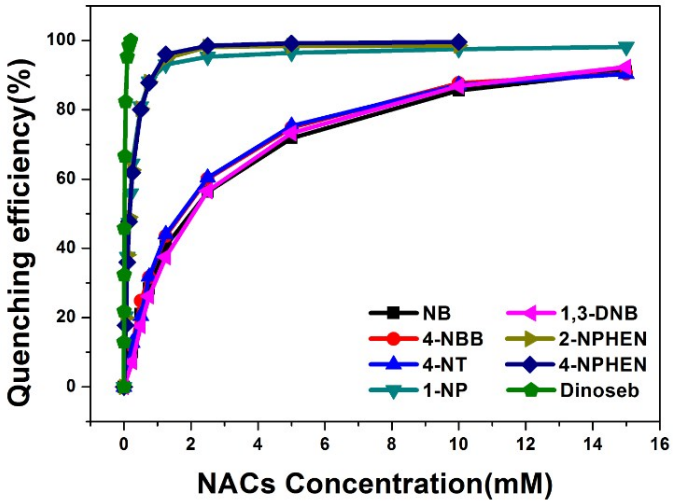

Fig. S26 Plot of quenching efficiency of **2** (a) dispersed in DMF upon incremental addition of different NACs.

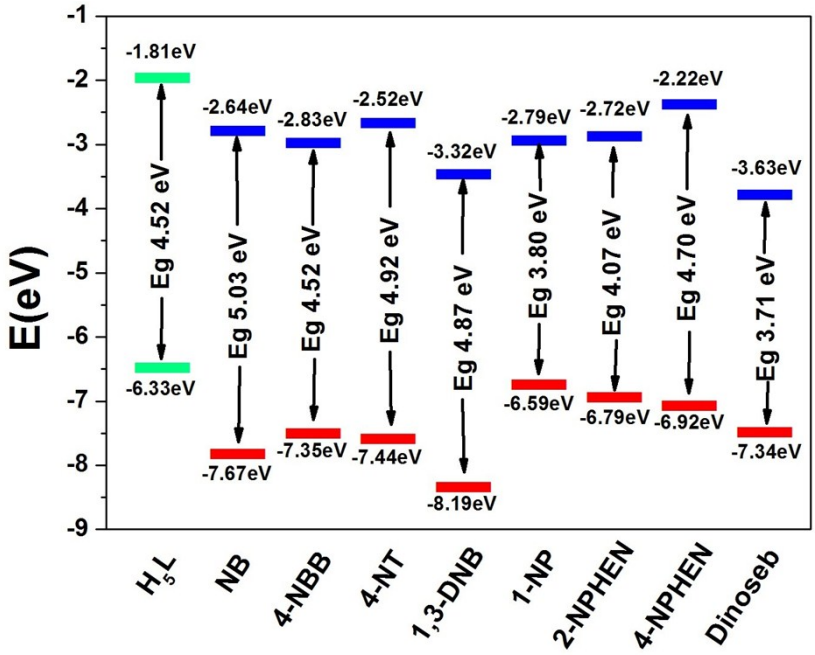

Fig. S27 The HOMO and LUMO energy levels for all the NACs and H_5L.

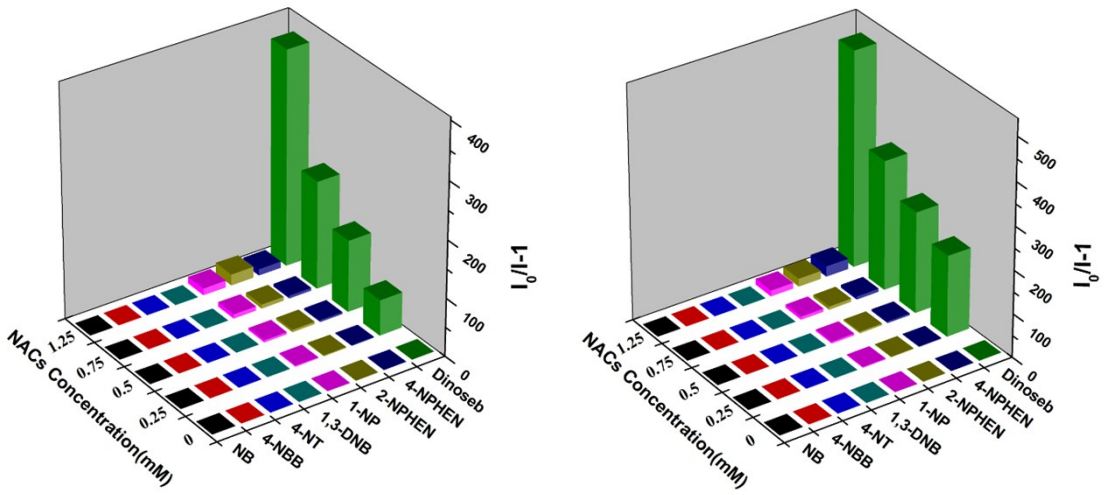

(a) (b)

Fig. S28 The Stern-Volumer Plots of **1** (a) and **2** (b) dispersed in DMF upon incremental addition of different NACs.

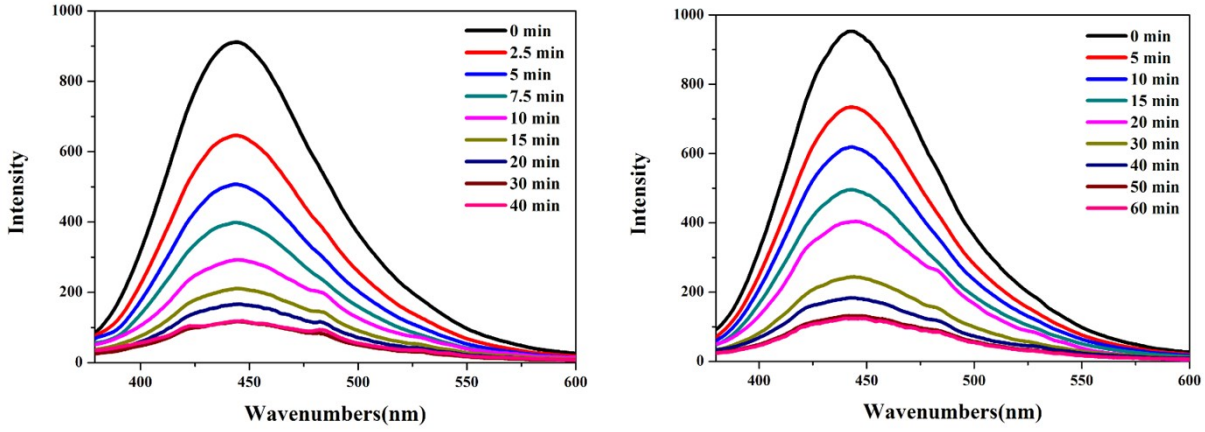

(a) (b)

Fig. S29 Time dependent fluorescence spectra of solid sample of **1** upon exposure to (a) NB and (b) 4-NT vapor.

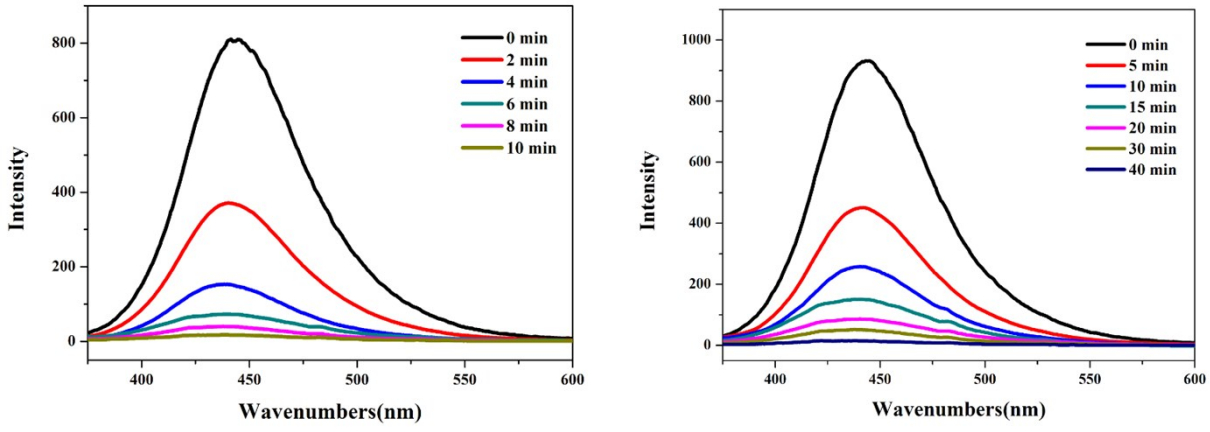

(a) (b)

Fig. S30 Time dependent fluorescence spectra of solid sample of **2** upon exposure to (a) NB and (b) 4-NT vapor.